Vacancy mediated magnetization and healing of a graphene monolayer

E. Nakhmedov,[1,2] E. Nadimi,[3] S. Vedaei,[3] O. Alekperov,[2] F. Tatardar,[2,4] A. I. Najafov,[2] I. I. Abbasov,[5] and A. M. Saletsky[6]

[1]*Faculty of Physics, Moscow State University, Baku Branch, Str. Universitetskaya 1, AZ-1144 Baku, Azerbaijan*

[2]*Institute of Physics, Azerbaijan National Academy of Sciences, H. Cavid Ave. 33, AZ1143 Baku, Azerbaijan*

[3]*Center for Computational Micro and Nanoelectronics (CCMN), Faculty of Electrical Engineering, K. N. Toosi University of Technology, Tehran, Iran*

[4]*Khazar University, Mahsati Str. 41, AZ 1096, Baku, Azerbaijan*

[5]*Azerbaijan State Oil and Industry University, Azadlig Ave. 20, Baku, Azerbaijan*

[6]*Faculty of Physics, Leninskie Gory 1-2, 119991 Moscow State University, Moscow, Russian Federation*

(Received 22 October 2018; revised manuscript received 4 January 2019; published 18 March 2019)

Vacancy-induced magnetization of a graphene layer is investigated by means of a first-principles DFT method. Calculations of the formation energy and the magnetization by creating the different number of vacancies in a supercell show that a clustering with a big number of vacancies in the cluster is rather favorable to that of isolated vacancies, homogeneously distributed in the layer. The magnetic moment of a cluster with a big number of vacancies is shown to not be proportional with the vacancy concentration, which is in good agreement with the recent experimental results. Our studies support the idea that, although the vacancies in graphene create a magnetic moment, they do not produce a magnetic ordering. It is shown that, although the Lieb's rule for the magnetization in a hexagonal structure violates, two vacancies, including a di-vacancy, in the supercell generates a quasilocalized state when they belong to the different sublattices and, instead, two vacancies generate an extended state when they belong to the same sublattices. Analytical investigation of the dynamics of carbon atom and vacancy concentrations according to the nonlinear continuity equations shows that the vacancies, produced by irradiation at the middle of a graphene layer, migrate to the edge of the sample, resulting in a specific *"segregation"* of the vacancy concentration and self-healing of the graphene.

DOI: 10.1103/PhysRevB.99.125125

I. INTRODUCTION

Investigation of graphene, the single two-dimensional (2D) sheet of graphite, is one of the priority directions among allotropic modifications of carbon and related nanostructures due to its topological properties. Unusual properties of pristine graphene such as ballistic electron propagation with extremely high carrier mobility of $\mu_e = 10^4$ cm^{2}V^{-1}s^{-1} at room temperature [1,2], existence of massless, chiral low-energy excitations, characteristic to Dirac fermions, observation of anomalous integer quantum Hall effect, even at room temperature [3], makes it an attractive material for the electrotechnical industry. Recent experimental and theoretical investigations show that a graphene sheet with vacancies heals itself under thermal annealing or electric potential spanning [4–16], so the vacancies either migrate toward the crystal edge or form a big hole near extended defects like grain boundary or dislocation in the crystal. This property of the graphene may have a great impact on the graphene-based electronic technology.

Defects engineering may enormously change kinetic and magnetic characteristics of graphene, extending a scope of its application in spintronics. The defects are usually produced as point defects, like substitutional and interstitial impurities and vacancies, either in the fabrication processes of a sample or by means of external factors, such as radiation or heavy-ion bombardment and chemical doping of a sample (see, e.g., Ref. [17] for a review). The vacancies are formed in a crystal by reconstruction of the lattice as a result of the knock-on of carbon atoms from the graphene lattice or/and as a result of bond rotations, e.g., the formation of Stone-Wales (55–77) and eight-ring defects, under bombardment with high-energy particles. A beam of high-energy particles acts as a local heat source and thus helps to overcome the defect formation energy barrier. Note that a class of the carbon-based materials has been experimentally revealed [18], which has a nanoporous structure and it is catalycally active. The nanoporous carbon is less ordered than graphite but not completely amorphous. Theoretical studies have shown [19] that an introduction of nonhexagonal rings by means of vacancies into carbon structure is the most likely method to get a nanoporous carbon structure.

Although many effects observed in graphene are attributed to the presence of vacancies and defects, we will particularly focus here on a magnetic response and self-repairing of graphene in the presence of vacancies.

Magnetic response associated with vacancies produced by the irradiation of graphene with high-energy protons and carbon (C^{4+}) ions has been studied recently experimentally [20–22] as well as theoretically [23–29] by means of molecular dynamics simulations and density-functional-theory (DFT)-based *ab initio* methods. Many experimental observations reported in the literature provide inconsistent, even contradictory results. Experimental evidence of ferromagnetic order has been observed [21] in irradiated graphene,

the origin of which was suggested by the authors to be the defects located in the structure. Magnetic ordering was mainly observed in graphitic materials [22], which was explained by the existence of the localized electronic states at grain boundaries of highly oriented defective pyrolytic graphite. Some observation of ferromagnetism, even antiferromagnetism, seems to be an artifact.

Ab initio DFT investigations of magnetization produced by vacancies in graphene are mainly performed [19,24–30] by a superlattice method, where a vacancy is created in a supercell of the big number of unit cells, periodically extended with images of the original vacancy. Spin orientations in each supercell become the same, yielding seemingly a ferromagnetic signature of total magnetization even in the absence of spin-spin interactions. Nevertheless, we believe that a magnetic ordering in a system should be achieved by exchange interactions between the magnetic moments. A numeric computation reveals that a vacancy in graphene [20,31,32] introduces a semilocalized π-midgap state with Coulomb-like $\sim 1/r$ decay potential. The single-atom defects create in the graphene a quasilocalized state at the Fermi level [32–35]. The graphene structure can be viewed as two interpenetrating hexagonal sublattices of carbon atoms labeled as A and B, forming a bipartite lattice. A defect introduced into the A sublattice results in a quasilocalized state due to the p_z orbitals of carbon atoms in the B sublattice and vice versa. A short-range repulsive Hubbard interaction between vacancies at higher concentrations and with half-filled band may result in a ground state with total spin $S = |N_A - N_B|/2$, according to Lieb's theorem [36], where N_A and N_B are the number of vacancies in A and B sublattices, correspondingly, of a bipartite lattice. The balance between N_A and N_B is destroyed at, e.g., zigzag edges, which may provide a low-temperature background magnetism observed in a graphene sample [37].

Recent investigation of a graphene sheet by controllable doping with fluorine adatoms and creation of vacancies by irradiation [38–40] has indicated that both defects induce magnetic moments with spin 1/2. Nevertheless, they do not result in a magnetic ordering, rather an induced paramagnetism down to liquid helium temperatures was observed in the doped samples. Low-temperature measurements of pristine graphene using SQUID magnetometry disclose strong diamagnetism [40], and show a tiny background paramagnetism, observable at $T < 50$ K. The samples under investigation were shown [38,40] to consist of electronically decoupled 10−50 nm mono- and bilayer graphene crystallites, which are aligned parallel to each other. Evaluation of the spin number N from the measurement data shows that the number of paramagnetic centers is proportional to the defect concentration x for a small concentration ($x < 0.5$), and the dependence is more complicated for higher concentrations. For each concentration x, the measured number of paramagnetic centers is three orders of magnitude less than the measured number of defects in the samples. This experimental fact can be understood such that only one of out $\sim$1000 defects contributes to the paramagnetism in contradiction to other experiments as well as ab-initio investigations [19,24–27,29] that each defect contributes one Borh magneton μ_B to the total magnetization. Note that the vacancy magnetism in graphene was recently shown [39] to have originated from two approximately equal contributions: one from the dangling bonds and the other from itinerant magnetism.

High-resolution transmission electron microscope (HRTEM) monitoring of a graphene sheet at 80 keV operating energy has displayed [4] a formation of a hole, which seems to support the above described experiment [38] on vacancy magnetism. Indeed, as we will show, agglomeration of the vacancies in a big hole doesn't result in a linear increase of the magnetic moment with vacancy concentration. Theoretical investigations of time-evolution of graphene with dense vacancies by means of nonequilibrium molecular dynamics [5] also reveal a tendency toward a formation of the haeckelites in the case with a small number of the vacancies, while forming a large hole as the number of vacancies increases.

A systematic scanning transmission electron microscopy (STEM) study of a suspended graphene layer [6,7], deliberately introduced vacancies, and deposited by metal atoms such as Cr, Ti, Pd, Ni, Al except for gold, shows that nanoscale holes were etched in the structure due to interactions of metal atoms with graphene. The nanoholes were observed at room temperature in ultrahigh vacuum (6×10^{-9} mbar) under low-energy 60 keV (lower than the threshold "knock-on" energy 86 meV for a carbon atom [8] in graphene) that electron-beam scanning acts as catalysts for etching holes on the graphene surface. Instead, the mending and filling of many-vacancy holes (over 100 vacancies) was observed [9] in room-temperature metal-catalyzed etching STEM experiments under the same conditions described above, provided a reservoir of loose carbon atoms is readily available from nearby holes. This process was interpreted by the authors as a dislodging of carbon adatoms from the graphene surface by the scanning electron beam and dragging them to the edge of the holes, which results in refilling the holes by random combination of five, six, seven, and eight carbon atom rings.

Healing effect in graphene, where the vacancies were produced by employing plasma bombardment [10], has been performed by thermal annealing without an external carbon atoms source in the temperature interval starting from 300 °C up to 900 °C. For higher temperatures the self-repairing was shown to stop. According to the results of Raman, x-ray photoemission spectroscopy (XPS), HRTEM, and electrical transport measurements, the healing takes place by annihilation of displaced carbon atoms with vacancies with the assistance of thermal energy. Healing was shown to become more difficult when the size of the vacancy's hole increases. Formation of monovacancy defects in the finite graphene flakes [11] and graphene nanoribbons [12] was shown to be size-dependent, and that the vacancy defects migrate toward the edge at higher temperatures, as a result of which the structures heal themselves. DFT calculations and molecular dynamics simulations of the vacancy migration in graphene flakes show [13] thermally activated motion of vacancy toward the edge occurs even at room temperature whereas the probability of return motion back to the middle is negligible.

Our *ab initio* investigation of the vacancies and analytical study of their migration in a graphene layer supports the experimental results on magnetism measured in Ref. [38] as well as the experiments on self-healing of graphene. Analysis

of our calculation results shows that the formation energy and magnetization of divacancy (DV) is lower than those of single vacancies. Single vacancies are mobile enough, and they diffuse toward the extended defects like a grain boundary, a dislocation, or a sample edge (which can be considered as an extended defect), or coalesce with other vacancies, forming polyvacancies with lower energy and magnetic moment. We show that a merging of a single vacancy with polyvacancies, resulting in a defect cluster or a hole with a bigger size, is energetically favorable. According to our calculations, the formation energy of an even-fold vacancy like di- or tetravacancy is lower than odd-fold vacancies. Therefore, they are more stable. Magnetic moments of the clusters with minimal formation energies are lower too. The magnetic moment of the graphene is determined by the edge structure of the vacancy clusters, so only the defect on the, e.g., A sublattice that has no counterpart on the B sublattice will contribute to the magnetization. The authors of Ref. [12] considered a hole of $N > 1$ multiple vacancies, concluded that the dangling bonds these structural defect is proportional to the circumference of the hole or to $\sqrt{N}$, and therefore its formation energy is also proportional to $\sqrt{N}$. In contrast, we show that a multiple vacancy hole is structured in different modifications, and at least one of them possesses minimal dangling bonds and, consequently, minimal magnetic moment. Thus, there is a tendency of clustering of vacancies into big holes, instead of homogeneous distribution of isolated vacancies over the system in the irradiation process. It is worth noting that total energy calculations have been done in Ref. [30] for nanoholes of various sizes, containing up to 60 vacancies, in a big supercell with 288 carbon atoms in graphene by applying *ab initio* DFT method. Although the number of possible holes for a given number vacancies N increases sharply with N, it is hard task to calculate all possible cluster structures with higher N. Nevertheless, the results of Ref. [30] yield extremely useful information on stability and magnetism of holes with a great number of vacancies.

Such kind of "*segregation*" seems to be a result of the 2D character of the graphene sheet, where an off-diagonal long-range order (ODLRO) is absent. The crystalline structure of the graphene is controlled by powerlike order. Correlations of the vacancies seem to also be managed with powerlike order, which compete with correlations between the carbon atoms in the structure. To understand the vacancy hole formation and healing mechanism in a graphene layer, we employ a phenomenological kinetic model for a migration of carbon atoms through vacancies. This model has been implemented in numerical studies of a segregation problem under irradiation of binary alloys [41–51], where A- and B-type atoms diffuse over vacancies and interstitials. We simplified the segregation problem for diffusion of carbon atoms over vacancies in the one-dimensional (1D) case and solved analytically the nonlinear differential equations for carbon atoms and vacancy concentrations. The obtained results show that a vacancy created, say, in the middle of the sample, diffuses to the edge of the sample. We think that boundary of samples can be considered an "extended defect" like dislocations, grain boundaries, or a hole of a big size. Therefore, the vacancies diffuse and are incorporated commonly, say, around extended defects in the sample.

TABLE I. Formation energies of mono-, di-, and trivacancy for the supercells with 50, 98, and 162 atoms.

Formation energy (eV)	One vacancy	Two vacancies	Three vacancies
Supercell with 50 atoms	7.03	5.78	8.50
Supercell with 98 atoms	6.99	5.76	7.74
Supercell with 162 atoms	6.78	5.21	7.52

The paper is structured as follows: The computational method employed for our *ab initio* calculations is described in the Sec. II. Section III presents the obtained results of *ab initio* DFT calculations. Section IV provides our analytic investigation of the diffusion-segregation problem for carbon atoms through vacancies and migration of the vacancies toward the sample boundary. Our conclusions and speculations are given in Sec. V.

II. COMPUTATIONAL METHODS

SIESTA code is employed [52,53] in our spin-polarized DFT-based *ab initio* calculations, where the standard double-ξ basis with polarization orbitals is used. The generalized-gradient approximation is utilized to calculate the exchange correlation term [54]. The interaction between the valence electrons and the atomic core is taken into account by using standard norm-conserving Troullier-Martins pseudopotential. The unit cell of a pristine monolayer graphene is initially relaxed and then three different supercells of 50, 98, and 162 atoms are constructed. The real-space integration grid had 200 Ry cutoff and 50 meV energy shift. Spin-resolved calculations are performed in most cases. k-point sampling of the Brillouin zone was performed by using the Monkhorst-Pack method [55]. To get an optimal self-consistency convergence, the density of electronic states (DOS) was calculated for different k-point meshing. Our calculations show that $5 \times 5 \times 1$ k-point mesh is a good and optimal choice to have a balanced accuracy and computation time. To obtain the equilibrium geometry, we relaxed all the atoms after creating each vacancy until the forces acting on them were smaller than $0.01\,\mathrm{eV/\AA}$. The formation energy for mono-, di-, and trivacancy are presented in Table I for the supercells with 50, 98, and 162 carbon atoms. The formation energy of the vacancies changes slightly with the supercell size (see Table I) as a result of interaction of the defects with their images in the neighboring auxiliary cells (we used periodic boundary conditions in all space directions). Our calculations of the formation energy, DOS, and the magnetization show that a good convergence can be reached for a supercell with at least 98 atoms. Therefore, our results presented below were done for a supercell with 98 atoms.

III. DISTRIBUTION OF THE VACANCIES AND THEIR MAGNETIZATON

Our aim in this investigation is to understand a development of the magnetization with increasing the vacancy concentration and a restructuring tendency due to the vacancies' migration in the graphene monolayer. We calculated for this

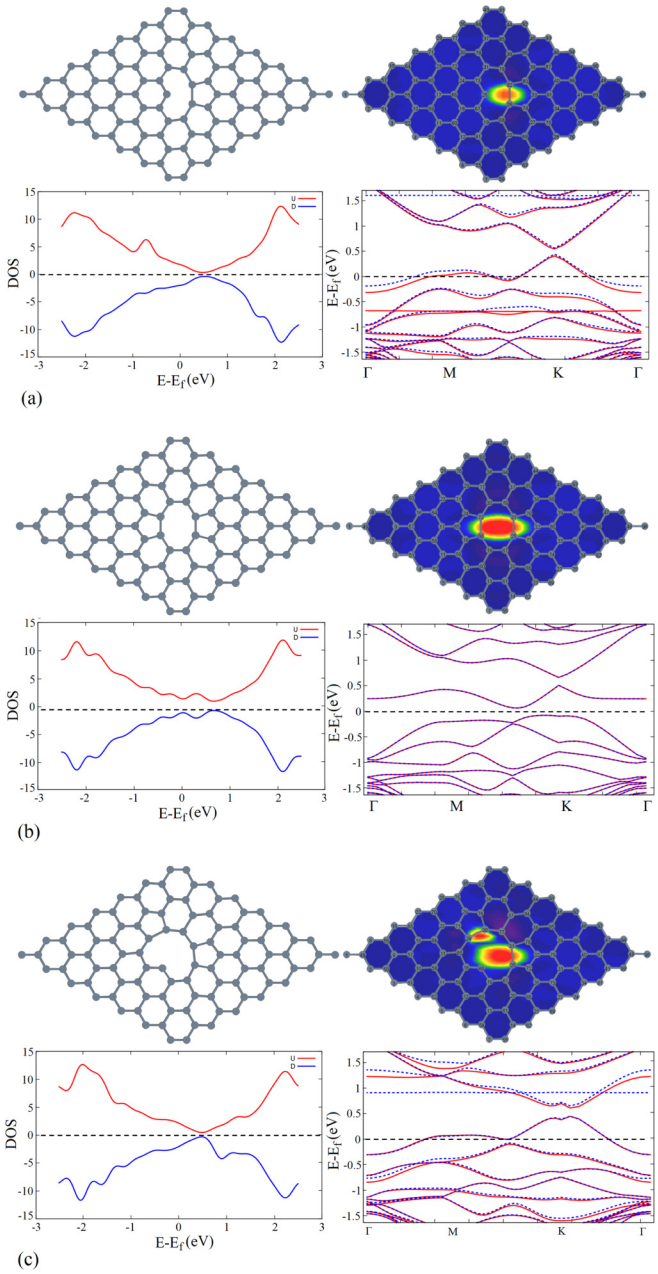

FIG. 1. The relaxed structure and the deformation potentials around the vacancies, the spin-polarized DOS, and the band structures for (a) mono-, (b) di-, and (c) trivacancy, when one carbon atom or two and three nearest-neighboring carbon atoms are removed in the unit cell. The DOS, corresponding to spin-up and spin-down states, are plotted, respectively, by red and blue curves in opposite directions for clarity.

purpose the formation energy, the band structure, and the DOS of a supercell of 98 atoms with up to four vacancies in different configurations. The C–C bond length of a pristine graphene lattice is calculated to be 1.409 Å, 1.412 Å, and 1.412 Å for the supercells, correspondingly, with 50, 98, and 162 atoms, which is in good consistency with the experimental value of 1.42 Å. Creation of one vacancy, producing pentagon-nonagon type 5-9 defect in the supercell, results in the appearance of three dangling σ- bonds, two of

TABLE II. Formation energy and total spin polarization for the supercell of 98 atoms with different vacancies.

Type	Formation energy (eV)	Spin polarization ($Q_{\text{up}} - Q_{\text{down}}$)
Single defect	6.99	1.13
DV 5-8-5	5.76	0.0
DV 555-888	4.52	0.0
3 vac. 55-10	8.84	1.00
3 vac. 999-3	17.49	4.00
3 vac. 555-11	11.91	1.54
4 vac. 555-9	7.91	0.0
4 vac. 5-12-5a	11.27	2.02
4 vac. 5-12-5b	11.27	2.02
4 vac. 55-12	13.33	1.99
4 vac. 12-55	13.33	1.99

which rebind again with each other due to the Jahn-Teller distortion around vacancy. Jahn-Teller distortion deforms the lattice around the vacancy and breaks the threefold symmetry; the geometrical distortion is relaxed off behind the vacancies. Covalent-bond coupling between two dangling bonds of the second-nearest-neighboring atoms belonging to the same sublattice stabilizes the vacancy extended states. The third dangling bond is left unsaturated and contributes $\approx 1\,\mu_B$ in magnitude magnetic moment to the intrinsic magnetization. Removing one-, two-, and three-carbon atoms located in the nearest-neighboring sites in the unit cell results in formation of, correspondingly, 5-9, 5-8-5, and 55-10-type defective configurations in the supercell (see Fig. 1). DOS, the band structure, and the distributions of the deformation potential around the mono-, di-, and trivacancy distortions are depicted in Fig. 1. The deformation potential is seen to be significant within the unit cell around the vacancy. Therefore, interaction of vacancies through the distortion potential seems to be like the dipole interaction and it would be important only for vacancies placed nearest neighbor to each other. The vacancies located far away from each other may be considered practically as isolated vacancies. Formation energy of a single vacancy is calculated to be 6.99 eV (see Table II). This result is slightly lower than those obtained by other authors $E_f \approx 7.5$ eV [29,56,57], nevertheless it is in good consistency with the experimental data of 7.0 ± 0.5 eV [58]. The spin-polarized electronic band structures of a defective graphene with one vacancy and a pristine graphene are shown in Figs. 1(a) and 2(a), correspondingly, for comparative study. The band gap of the perfect graphene is closed at the border of the Brillouin zone, yielding two Dirac cones. A single vacancy seems to remove the band crossing degeneracy at K-points of the Brillouin zone, and introduces at the same time two extended defect levels corresponding to spin-up and spin-down states at the Fermi level. Assuming that a continuous irradiation of a sample will create isolated vacancies, the magnetization of the sample would monotonically increase. Furthermore, in the absence of spin-spin correlations between localized dangling bonds, the magnetic moments of the vacancies belonging to different sublattices will partially compensate each other and reduce the total magnetization. Nevertheless, the magnetization under this assumption would

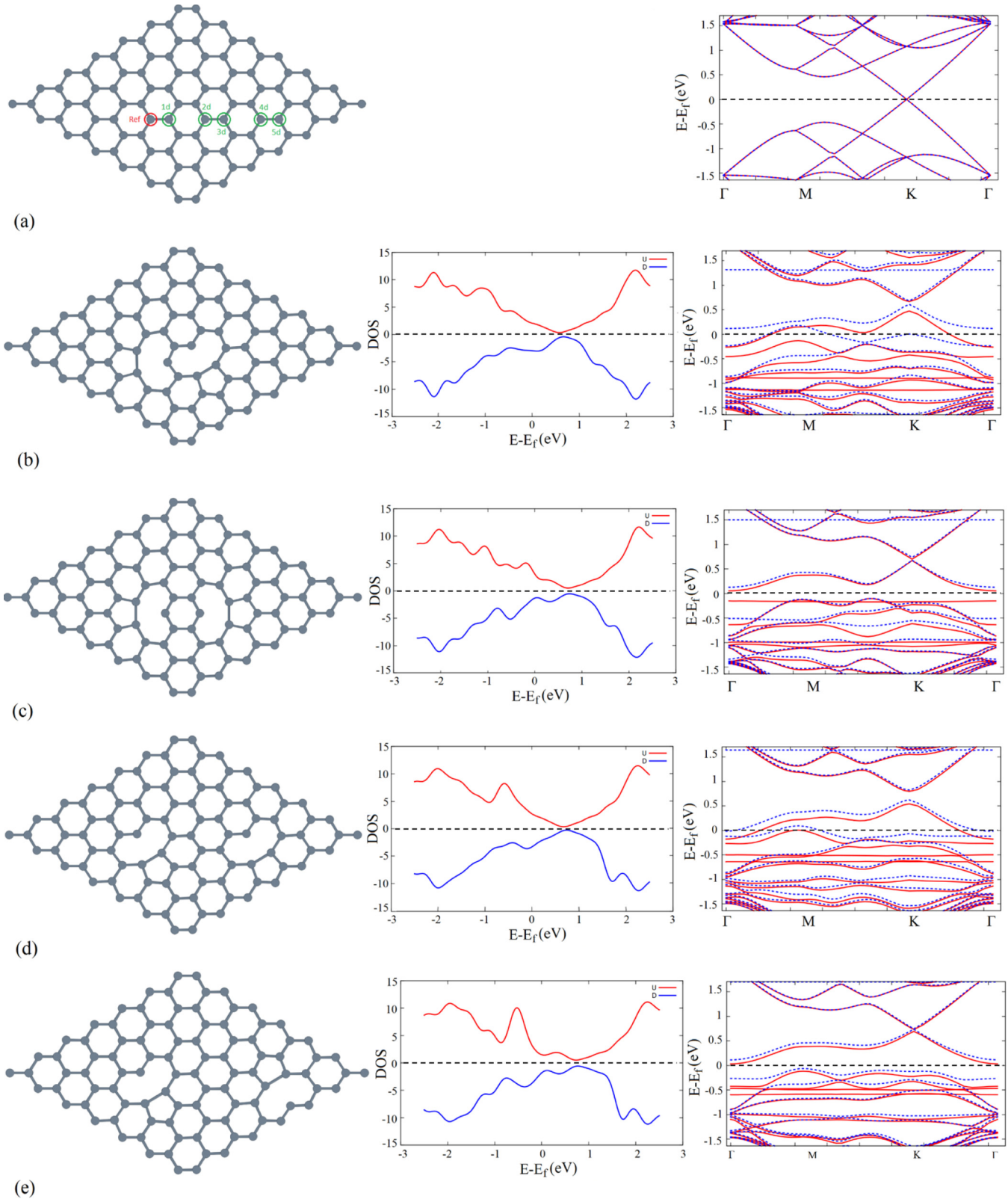

FIG. 2. (a) Band structure of a pristine graphene monolayer and a supercell of two-vacancy states, produced by removing a reference (red circle) and second C atoms 1, 2, 3, and 4 (green circles) located, correspondingly, in the 1d, 2d, 3d, and 4d interatomic distances with d being equal to C—C bond length. The relaxed supercell, DOS, and the band structure of two vacancies located at (b) one atomic distance (1d), (c) 2d, (d) 3d, and (e) 4d interatomic distances.

monotonically increase with vacancy concentration. Our calculations below show that creation of monovacancies monotonically distributed throughout the structure are not energetically favorable, and there is a tendency to form a cluster or hole of vacancies by coalescing them to each other or collapsing around the extended defects like grain boundaries, dislocations, or the sample boundary.

A DV is produced by the removal of two nearest-neighboring carbon atoms, composing the so-called *5-8-5* defect of an octagon and a pair of pentagons as shown in Fig. 1(b). We calculated the formation energy of DV, presented in Table II, which is equal to $\epsilon^f_{\rm DV} \approx 5.76$ eV. *Ab initio* calculations of the DV formation energy by other authors [56,57] indicate ∼8 eV. The energy $\epsilon^f_{\rm DV}$ is smaller than that for a monovacancy in graphene, confirming that DV formation in the graphene is rather favorable. Divacancies create a quasilocalized state with energies close to the Fermi energy E_F; at the same time, they remove the band crossing, destroying the gapless states at K-points of the Brillouin zone [see Fig. 1(b)]. All the dangling bonds corresponding to the same sublattice rebind again, and therefore the DV does not generate a magnetization (see Table II).

The 5-8-5 DV, consisting of two pentagons and one octagon, has another modification, 555-777, which is structured by three pentagons and three heptagons. The 555-777 defect is formed by removing two carbon atoms and by additional creation of a Stone-Wales defect [59], e.g., by additional rotation of one C—C bond in the octagon.

Although 555-777 DV, with formation energy smaller then that for monovacancy (see Table I), is suggested [60] to be more stable, 5-8-5 DV is responsible for migration of DV. *Ab initio* calculations in Ref. [60] show that subsequent transformations of 555-777 DV into 5-8-5 then 5-7-7-5 and again 5-8-5 DV finally create 555-777 DV, which differs from the initial one by rotation. 5-8-5 DV transforms to two sequential 5-7-7-5 metastable DV structures, which differ from each other by rotation of heptagons and shifting of pentagons. The metastable 5-7-7-5 DV structure finally turns to stable 5-8-5 DV, the position of which differs slightly from the position of the initial 5-8-5 DV.

To see clearly the differences between a DV and other possible two-vacancy structures, the latter are created, as seen from Fig. 2, in four different positions within the supercell, belonging both to the same or to different sublattices. Note that study of the two-vacancies problem is an instructive one to understand Lieb's rule and the contribution of the dangling bonds to the magnetization.

Two removal vacancies' positions in the supercell are depicted in Fig. 2(a), where the vacancies at "even distance" and the reference vacancy, shown in red, belong to the same sublattice [see Figs. 2(b) and 2(d)], instead of the "odd distance" vacancy and the reference vacancy belong to the different sublattices [see Figs. 2(c) and 2(e)]. According to the Lieb's rule, the magnetization in the first case should be finite, whereas in the second case it should be zero. The formation energies and the magnetizations of different two-vacancy topologies are presented in Table III. As seen from Fig. 2, all relaxed supercell structures contain two pentagon-nonagon *5-9* defects, each of which is typical of a monovacancy in Fig. 1(a), even when two vacancies are located in 1d distance.

TABLE III. The formation energy and the total spin polarization for two vacancies in different positions shown in Fig. 2.

Distance (in interatomic dist. d)	Formation energy (eV)	Spin polarization ($Q_{\rm up} - Q_{\rm down}$)
1d (DV)	5.76	0.0
2d	13.027	2.614
3d	13.197	2.003
4d	13.547	2.339
5d	13.435	2.016

Two vacancies in larger distance do not interact practically with each other, and the formation energies as well as the magnetizations become approximately two times higher than that of a monovacancy. All the two-vacancy structures (in Fig. 2), except a DV in Fig. 1(b), have dangling bonds. Consequently, the local DOS of DV for spin-up and spin-down states, shown in Fig. 1(b), correspondingly, by red (above zero) and blue (below zero) curves, coincides completely at each point. The local DOS corresponding to two opposite spin polarizations for all other vacancy configurations, presented in Fig. 2, differ from each other due to existence of the dangling bonds. The magnetization of all these configurations becomes nonzero irrespective to which sublattice the vacancies belong. This fact shows that the Lieb's rule seems to violate for a graphene monolayer, and the magnetic moment of the supercell with several vacancies is determined with the number of the dangling bonds but not with the difference of the number of atoms in each sublattice. The band structures of DV and all other two-vacancy states are presented, correspondingly, in Figs. 1(b), and Figs. 2(b)–2(e). It is necessary to pay attention to the fact that two vacancies (including the DV) generate a quasilocalized state [see the band structures in Figs. 1(b), 2(c), and 2(e)] when they belong to the different sublattices, and instead two vacancies generate an extended state (see the band structures in Figs. 2(b) and 2(d) when they belong to the same sublattice. Furthermore, the band structures, corresponding to spin-up and spin-down states, coincide with each other only in the presence of the DV due to absence of a dangling bond. All other two-vacancy structures contain dangling bonds, resulting in a splitting of opposite spin-polarized states in the band structures.

To create a trivacancy structure, we remove three nearest-neighboring carbon atoms belonging to one hexagon in the center of the supercell. The relaxed structure, depicted in Fig. 1(c), creates a 55-10 defect consisting of two pentagons and one decagon. The band structure and DOS of graphene with a trivacancy defect is presented in Fig. 1(c). Trivacancy introduces four defect levels, two of which narrow back the band gap and other two levels cross the Fermi level, transforming the graphene to a metallic state. Apart from the trivacancy defect, two other structures with three vacancies are considered, which are produced (i) by removing two nearest-neighboring carbon atoms in a hexagon but the third one is located in the next-nearest to these two atoms as depicted in Fig. 3(a), producing three pentagon and one undecagon defect, and (ii) by removing three carbon atoms in a hexagon all belonging to one sublattice as shown in Fig. 3(b), which produces three nonagon and one triangle. All these

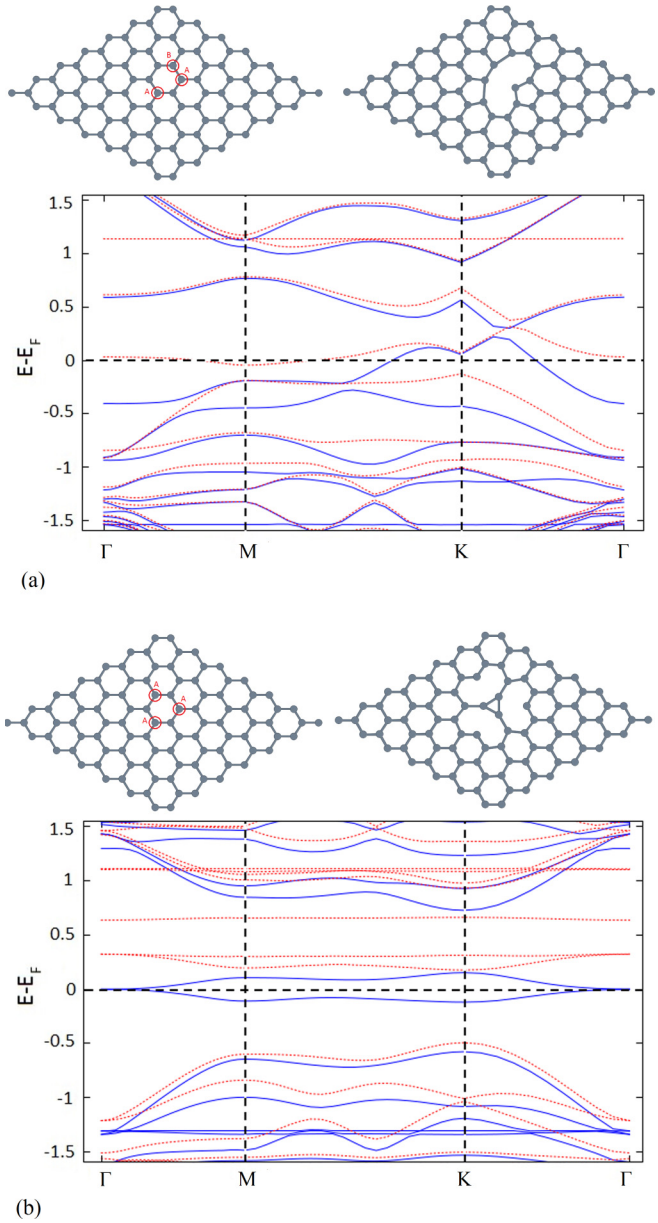

FIG. 3. Two other possible structures for three-vacancy defect, where all three vacancies are not bounded to each other, which is different from the trivacancy structure in Fig. 1(c) with three bounded removal C atoms.

configurations with three vacancies contain dangling bonds, and therefore, reveal a magnetic moment. Nevertheless, the formation energy and the magnetic moment of the trivacancy of 55-10 defect take the values 8.84 eV and 1.00 μ_B, correspondingly (see Table II). The values of the formation energy and the magnetic moment for other configurations 999-3 and 555-11 are, respectively, 17.49 eV, 4.00 μ_B and 11.91 eV, 1.54 μ_B (see Table II), which are much higher than those given for trivacancy 55-15. The tetravacancies of different configurations are depicted in Fig. 4. Among of all these configurations, only one structure, 555-9, containing three pentagon and one nonagon defects, has the minimal formation energy 7.91 eV and zero magnetic moment (see Table II). The

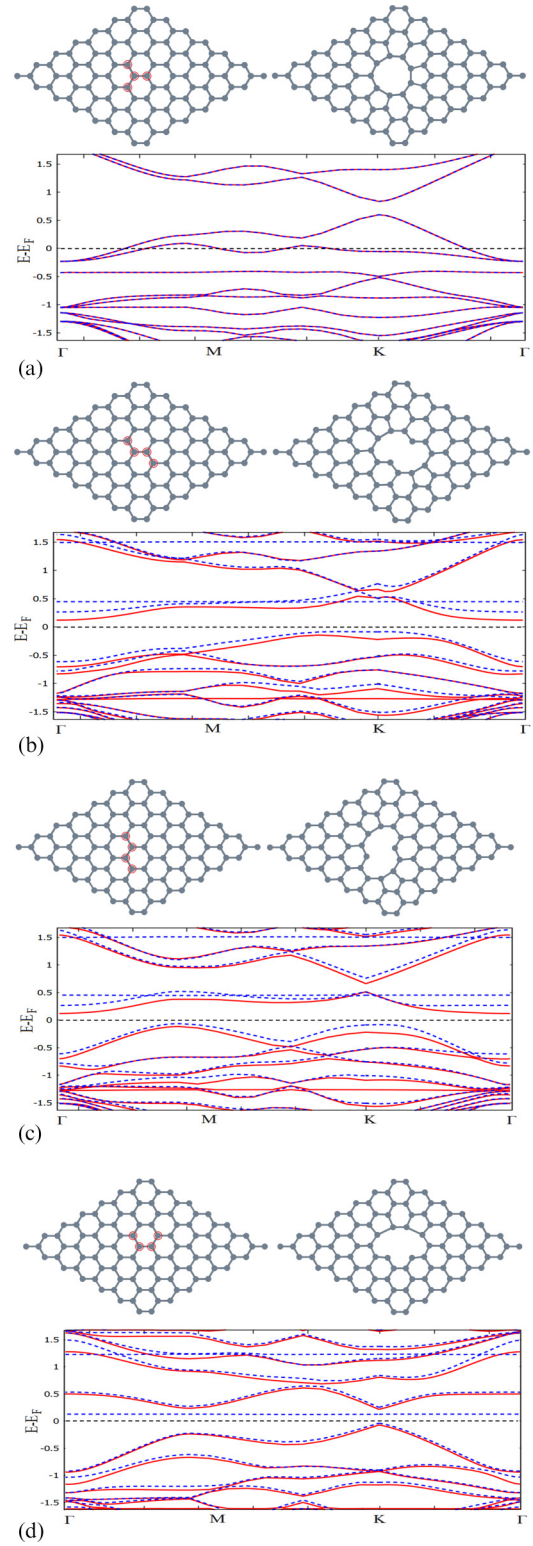

FIG. 4. Different topologies of four vacancies in the supercell, their band structures and the relaxed supercell. The removal atoms in the supercell are shown by the red circles.

relaxed supercell and the band structure of 555-9 tetravacancy is depicted in Fig. 4(a). The opposite spin-polarization bands of the 555-9 tetravacancy are highly degenerated. Furthermore, the Fermi energy in this case crosses the vacancy level

yielding an extended state. Two other tetravacancy configurations, the relaxed supercells, and the band structures of which are shown in Figs. 4(b) and 4(c), contain exactly the same defect structure 5-12-5 of two pentagons and one dodagon and have the same formation energy ∼11.27 eV and the magnetic moment ∼2.02 μ_B. The tetravacancy structure 55-12 of two pentagon and one dodagon defects, presented in Fig. 4(d), is produced by removing four nearest-neighboring atoms in a hexagon. The same relaxed supercell with the 55-12 defect is obtained by removing two nearest-neighboring atoms on one side and two similar atoms on the other side of the hexagon so these pairs are not connected to each other. The formation energy and the magnetic moment of this type of defect are 13.33 eV and 1.99 μ_B, correspondingly. A small band gap is opened around the Fermi level in these configurations, the band structures of which are presented in Figs. 4(b)–4(d), yielding quasilocalized states. Note that there is an imbalance of the vacancies between the sublattices A and B in the tetravacancy depicted in Fig. 4(a), since three vacancies belong to one sublattice and only one vacancy belongs to the other sublattice. Nevertheless, the number of vacancies located in A and B sublattices are equal to each other in the other three tetravacancy configurations of Figs. 4(b)–4(d). Note that tri- and tetravacancy have been studied [61] by coalescing a monovacancy to di- and trivacancy, correspondingly. Therefore, the obtained morphologies correspond to those drawn in Figs. 4(b)–4(d) with nonzero magnetic moments.

The discussion above shows that SVs in graphene are rather mobile defects, which may migrate and coalesce with other single vacancies, forming a DV or with other polyvacancies even at temperatures slightly higher than room temperature. DVs are immobile defects at room temperature. Nevertheless, they can migrate either at higher temperatures or by means of transformation to other DV modifications. The mobile defects are reincorporated into the crystal structure at dislocations, grain boundaries, and other defect sinks or at the crystal external surfaces.

Summarizing all these calculation results, one can conclude that (i) among of the vacancy clusters with even vacancies, there is at least one cluster where the dangling bond is absent. The magnetic moment of such vacancy cluster is zero, and the formation energy of such cluster is less than those of all other clusters with the equal number of the vacancies; (ii) among of the clusters with odd vacancies, there is at least one configuration which contains only one dangling bond. The formation energy of such cluster is minimal among of all clusters with an equal number of vacancies, and the magnetic moment of this vacancy cluster in ∼1 μ_B; (iii) the vacancy induced magnetic moment of the graphene does not obey the Lieb's rule, which states that the magnetization of a bilattice structure is determined with the difference of the atomic number in the sublattices. Our calculations show that the vacancy-induced magnetic moment is determined with the number of the dangling bonds in the structure; and (iv) the formation energy of N vacancies coalescenced into a single hole is less than the other aggregations of N vacancies with several pieces. Therefore, monovacancies in graphene migrate and are collected in a holelike structure with lowest energy. In a real crystal, migration of mobile vacancies takes place toward extended defects existing in the structure like grain boundary, dislocation, or a sample edge, segregating from the parent structure and healing the crystal.

IV. SEGREGATION OF VACANCIES AND HEALING EFFECT IN GRAPHENE

Recent transmission electron microscopy (TEM) [62–65] and scanning tunneling microscopy experiments [66] reveal defects, vacancies, and their migration in graphene with atomic resolution. Irradiation of a graphene sample with high-energy electrons or ions creates homogeneously distributed single vacancies. The migration barrier of a single vacancy in graphene was calculated by several groups [56,57,61] yielding about 1.3 eV. We examined that a formation energy of DV is lower than that of two isolated monovacancies. This fact has been shown in other works [67,68] too. Therefore, the single isolated vacancy is rather mobile, and it can migrate and has a tendency to coalesce either with other single vvacancies to form a DV [67] or with an extended defect like grain boundary, dislocation, or the sample edge. The migration energy of a DV was calculated [56] to be around of 7 eV, which is much higher than that presented above for a single vacancy. Nevertheless, migration of the DVs has been recently reported in Girit *et al.* [64], where the real-time dynamics of carbon atoms were visualized in a defective graphene using the aberration-corrected TEM technique. The subatomic resolution of the TEM images allows us to observe a formation of DVs and their diffusion in the crystalline structure. In the previous section, we calculated a formation energy of three vacancies (in one hexagon) and four (connected) vacancies in the supercell, which can be realized in three and four different forms, depicted in Figs. 1, 3, and 4, correspondingly. Among these configurations, only trivacancy [Fig. 1(c)] and tetravacancy [Fig. 4(a)] have minimal formation energy and minimal magnetization, allowing the vacancies to inosculate into a big cluster.

Irradiation produces point defects, which are distributed randomly throughout the sample. The flux of atoms and defects causes a buildup or depletion of alloying defects and/or vacancies in the vicinity of dislocations, grain boundaries, or the crystal surface.

To study dynamics of atoms and defects in graphene, resulting in their redistribution, we use extensive kinetic model of segregation in dilute alloys [47,48,50,51]. The possibility that impurities or alloying elements might segregate and form second phases at internal surfaces such as voids or on the external surfaces during irradiation was reported in many publications [41–46,49–51] and was first confirmed experimentally in a high-purity 18Cr − 8Ni − 1Si stainless steel during *in situ* bombardment in a high-voltage electron microscope [42,43], in heavy-ion bombarded vanadium [44,45], stainless steels [46], and in nickel binary alloys [49]. The vacancies in the graphene layer are considered to be in a thermal equilibrium state during the diffusion process, which imposes that the thermal equilibrium concentration of the vacancies is reached in a time considerably smaller than the diffusion time. A diffusion process is characterized by the concentration gradient of the carbon atoms or the vacancies, which is the only factor of the nonequilibrium process.

As a consequence of irradiation of the graphene with ions (e.g., with fluorine) or with high-energy protons and carbon (C^{4+}) ions [38], the local concentrations of C_A carbon and C_B alloying atoms as well as the local concentrations of C_V vacancies and C_i interstitials change, according to the following continuity equations [46,49–51] for atoms or defects fluxes:

$$\frac{\partial C_A}{\partial t} = \nabla\,[D_A\alpha\nabla C_A + SC_A(d_{Ai}\nabla C_i - d_{AV}\nabla C_V)], \quad (1)$$

$$\frac{\partial C_V}{\partial t} = \nabla[-(d_{AV} - d_{BV})\alpha SC_V\nabla C_A + D_V\nabla C_V]K_0 - R, \quad (2)$$

$$\frac{\partial C_i}{\partial t} = \nabla[(d_{Ai} - d_{Bi})\alpha SC_i\nabla C_A + D_i\nabla C_i] + K_0 - R, \quad (3)$$

where K_0 and R are, correspondingly, the rates of production and recombination of vacancies and interstitials by irradiation, and S is the average surface area of the 2D sample under investigation. The first term on the right-hand side of Eq. (1) is the atom (carbon atom and adatom in our case) fluxes induced by the chemical-composition gradient, the second and third terms are the atom fluxes driven by the interstitial and vacancy gradients, respectively. The defect fluxes represented by the right-hand-side of Eqs. (2) and (3) for vacancies and interstitials are driven by the A- and B-atom concentration gradients and by their own gradients, respectively. The total diffusion coefficients for the various species D_A, D_B or D_V, D_i are written as [51]

$$\begin{aligned} D_A &= d_{AV}N_V + d_{Ai}N_i, \\ D_V &= d_{AV}N_A + d_{BV}N_B, \\ D_i &= d_{Ai}N_A + d_{Bi}N_B, \end{aligned} \quad (4)$$

where N_A (N_B) and N_V (N_i) are the A (B)-atom fraction and the atomic fraction of vacancies (of interstitials), respectively. The two terms in the expression of D_A are the partial diffusivity coefficients of A atoms, respectively, via N_V atomic fraction of vacancies and via N_i atomic fraction of interstitials. The diffusivity coefficients d_{AV} and d_{Ai} are given as [69]

$$d_{AV} = \tfrac{1}{4}b_V^2 z_V \nu_{AV}, \quad d_{Ai} = \tfrac{1}{4}b_i^2 z_i \nu_{Ai}, \quad (5)$$

where ν_{AV} (ν_{Ai}) is the jump frequency for the exchange of a given A-atom-vacancy (A-atom-interstitial) pair, b_V (b_i) and z_V (z_i) are, correspondingly, the jump distance and the coordination number for a vacancy (for an interstitial). The similar parameters can be defined for a diffusion of B atoms via interstitials and vacancies. The equation for the element B is omitted according to the relation $C_B = 1 - C_A$. The thermodynamic factor α in expressions Eqs. (1)–(3),

$$\alpha = 1 + \frac{\partial \ln \gamma_A}{\partial \ln N_A} = 1 + \frac{\partial \ln \gamma_B}{\partial \ln N_B}, \quad (6)$$

takes care of the difference between the chemical potential gradient [51], which is the true driving force for the diffusion of A and B atoms, and the concentration gradient. γ_A and γ_B are the activity coefficients. The thermodynamic factor deviates from unity for nonideal solutions.

The coupled system of Eqs. (1)–(3) is a set of *the nonlinear partial differential equations* in two variables, which was solved numerically in many works [42–46,49–51]. To study the dynamics of the vacancy concentration in graphene, we simplify expressions Eqs. (1)–(3), written forthe 1D case, by ignoring the interstitials ($C_i = 0$) and alloying atoms ($C_B = 0$), also by converting the surface concentrations C into the atomic fractions N according to the relationship $N_A = SC_A$ and $N_V = SC_V$. We assume that an irradiation of the system is finished, and further generation of the vacancies and defects is stopped, $R_0 = 0$ and $K = 0$. By turning to new dimensionless variables $\rho = x/b_V$ for the spatial coordinate and $\tau = z_V \nu_{AV} t/4$ for the time, the equations for the dimensionless atomic fraction $N_A = C_A S$ and $N_V = C_V S$ read as

$$\frac{\partial N_A}{\partial \tau} = \frac{\partial}{\partial \rho}\left[\alpha N_V \frac{\partial N_A}{\partial \rho} - N_A \frac{\partial N_V}{\partial \rho}\right], \quad (7)$$

$$\frac{\partial N_V}{\partial \tau} = \frac{\partial}{\partial \rho}\left[N_A \frac{\partial N_V}{\partial \rho} - \alpha N_V \frac{\partial N_A}{\partial \rho}\right]. \quad (8)$$

Migration of a vacancy throughout the crystal is realized by hopping of a carbon atom over the vacancy. Therefore, the time evolutions of the atoms and the vacancies are opposite each other. Equations (7) and (8) are second-order nonlinear coupled equations for $N_A(\rho, \tau)$ and $N_V(\rho, \tau)$. Furthermore, the atomic fractions for carbon atoms $N_A(\rho, \tau)$ and for vacancies $N_V(\rho, \tau)$ are linked according to

$$N_A(\rho, \tau) = 1 - N_V(\rho, \tau), \quad (9)$$

since the total concentrations of carbon atoms and vacancies at an arbitrary point is conserved in the absence of interstitials as well as of production and recombination of the vacancies under irradiation.

We introduce new coordinate $\xi = \rho + \tau$ and demand that N_A and N_V depend only on ξ, so $N_A(\rho, \tau) = N_A(\xi)$ and $N_V(\rho, \tau) = N_V(\xi)$. It is worth noting that such transformation resembles the *soliton* transformation for the Korteweg-de Vries (KdV) equation [70]. Then Eqs. (7) and (8) can be written under this assumption and the condition Eq. (9) in the following form:

$$\frac{\partial}{\partial \xi}\left\{\alpha(1 - N_A)\frac{\partial N_A(\xi)}{\partial \xi} + N_A\frac{\partial N_A(\xi)}{\partial \xi} - N_A\right\} = 0, \quad (10)$$

$$\frac{\partial}{\partial \xi}\left\{(1 - N_V)\frac{\partial N_V(\xi)}{\partial \xi} + \alpha N_V\frac{\partial N_V(\xi)}{\partial \xi} + N_V\right\} = 0, \quad (11)$$

Further, we will study only Eq. (11) for the vacancy fraction, and the solution for $N_A(\xi)$ can be determined according to Eq. (9). Integration of Eq. (11) yields

$$(1 - N_V)\frac{\partial N_V(\xi)}{\partial \xi} + \alpha N_V(\xi)\frac{\partial N_V(\xi)}{\partial \xi} - N_V = N_0. \quad (12)$$

This Eq. (12) is once more integrated, yielding

$$[1 + (1 - \alpha)N_0]\ln\left|\frac{N_A(\xi) + N_0}{N_0}\right| - (1 - \alpha)[N_A(\xi) + N_0] = \xi + N_1. \quad (13)$$

The constants N_0 and N_1 have to be determined from the boundary conditions. A 1D sample of the dimensionless length L is assumed to be free of the internal defects and sinks, so that segregation could occur only to the edge. The conditions are imposed to half of the sample because of the symmetry of the problem. The vacancy is assumed to be created at $t = 0$ at the center of the sample $x = 0$ with

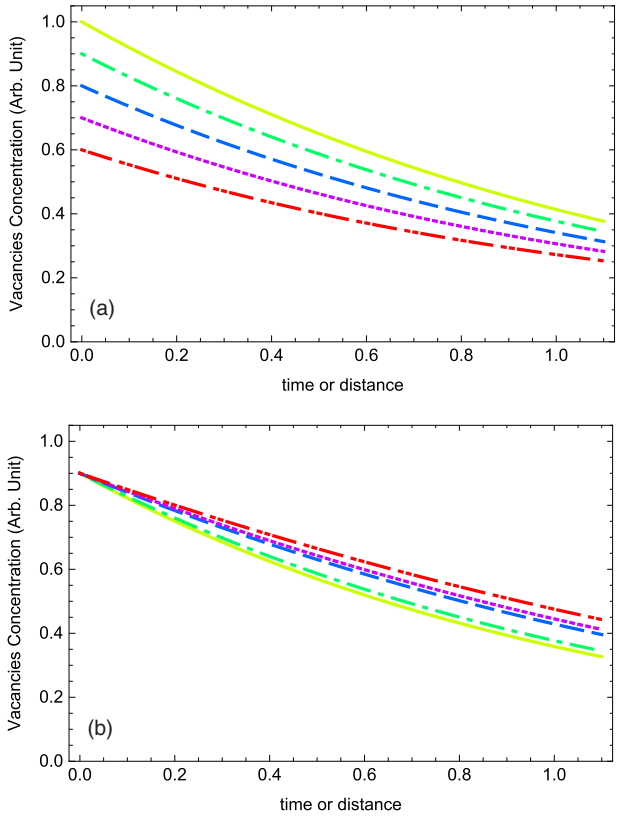

FIG. 5. Distribution of the vacancy concentration with time (or in space) in a sample with dimensionless length $L = 7$ (a) at fixed value of $\alpha = 1.2$ and for $N_{0V} = 1.0$ solid (yellow) curve, $N_{0V} = 0.9$ dot-dashed (green) curve, $N_{0V} = 0.8$ dashed (blue) curve, $N_{0V} = 0.7$ dotted (violet) curve, and $N_{0V} = 0.6$ double dot-dashed (red) curve; and (b) at fixed value of $N_{0V} = 0.9$ and for $\alpha = 1.1$ solid (yellow) curve, $\alpha = 1.2$ dot-dashed (green) curve, $\alpha = 1.5$ dashed (blue) curve, $\alpha = 1.6$ dotted (violet) curve, and $\alpha = 1.8$ double dot-dashed (red) curve.

concentration of $N_V(x = 0, t = 0) \equiv N_{0V} = \exp(-E_V/k_BT)$, where E_V is the formation energy of a vacancy. At the same time, the vacancy concentration and flux at the boundary $\xi = L/2$ is given as $N_V(\xi = L/2) = [1 - \exp(-E_V/k_BT)]/L = (1 - N_{0V})/L$ and $\frac{\partial N_V}{\partial \xi}|_{\xi=L/2} = 0$. These conditions yield

$$N_0 = \frac{N_{0V} - 1}{L} = \frac{1}{L}\left\{\exp\left(-\frac{E_V}{k_BT}\right) - 1\right\}, \quad (14)$$

$$N_1 = \left[1 - (1-\alpha)\frac{1 - N_{0V}}{L}\right] \ln\left|\frac{N_{0V} + \frac{N_{0V}-1}{L}}{\frac{N_{0V}-1}{L} + N_{0V}}\right| - (1-\alpha)\left(N_{0V} + \frac{N_{0V} - 1}{L}\right). \quad (15)$$

Finally, the time–plx-sol-plxcoordinate-evolution of $N_V(\xi = x/b_V + z_V v_{AV} t/4)$ reads as

$$\left[1 + (1-\alpha)\frac{N_{0V} - 1}{L}\right] \ln\left|\frac{N_V(x,t) + \frac{N_{0V}-1}{L}}{N_{0v} + \frac{N_{0V}-1}{L}}\right| - (1-\alpha)[N_V(x,t) - N_{0V}] = \frac{x}{b_V} + \frac{1}{4} z_V v_{AV} t. \quad (16)$$

Figure 5 shows the vacancy density dependence on time or coordinate. We assume that the vacancy concentration of $N_{0V}(T) = e^{-\frac{E_V}{k_BT}}$ is created at $t = 0$ at the middle of the sample $x = 0$ with length L by irradiation. Irradiation is stopped just at $t = 0$, and the system is relaxed to an equilibrium state by migration of the carbon atoms over the vacancies. Figure 5(a) shows migration of the vacancy concentration, created at $x = 0$ point at $t = 0$ with different concentration C_{0V} for fixed parameter α, with time, so that the vacancy concentration at $x = 0$ decreases with time and segregates to the boundary of the sample. Figure 5(b) displays the same dependence that is in Fig. 5(a) for fixed values of $C_{0V}(T)$ but for different values of α.

V. CONCLUSIONS

Considerable attention has been paid recently to understand magnetism of single-layered graphene. In this paper, we studied influence of the vacancies on the magnetic properties and healing effects of graphene. Our *ab initio* DFT investigations of mono-, di-, tri-, and tetravacancy in single-layer graphene show that the formation energy of many vacancies is lower when the vacancies coalesce together, forming a big cluster (hole) instead of homogeneously distribution over the structure as single vacancies. Furthermore, the formation energy is minimal when the σ-bonds, appearing in the process of vacancy creation, rebind each other, reducing the dangling bonds to the minimal number in the internal edge of the hole. In this case, a contribution to the magnetic moment yields the dangling bonds in the internal edge of the hole, the number of which is much less than the total number of the vacancies.

The process of clustering the vacancies is similar to the segregation process in binary compounds. In a crystalline binary bulk (3D) compound, the segregation may result in separation of the structure into two coexistent crystalline substructures or into film on the host crystal in the compound. Such a picture of a clustering and forming the holes under irradiation, instead of homogeneous creation of vacancies in graphene, seems to be a result of the 2D character of the structure and absence of the ODRLO [71].

ODLRO fails in the 2D crystals due to the Mermin-Wagner theorem [71,72]. Characterizing the order in the crystalline structure by the order parameter $\Delta(\mathbf{r})$ at a point $\mathbf{r}$, ODLRO is determined by the correlator $\langle\Delta(\mathbf{r})\Delta(\mathbf{r}')\rangle$, which behaves as $\langle\Delta(\mathbf{r})\Delta(\mathbf{r}')\rangle = C\exp(-\frac{\xi^{(3D)}}{|\mathbf{r}-\mathbf{r}'|^{\alpha}})$ for 3D structures, where $C > 0$ and $\alpha > 1$ are constants, $\xi^{(3D)}$ is the coherence length, and as $\langle\Delta(\mathbf{r})\Delta(\mathbf{r}')\rangle = (\frac{\xi^{(2D)}}{|\mathbf{r}-\mathbf{r}'|})^{\beta}$ for 2D systems, where $\beta > 1$ is a constant and $\xi^{(2D)}$ is the coherence length. Although the correlator in the 3D system saturates at long distance $\lim_{|\mathbf{r}-\mathbf{r}'|\to\infty}\langle\Delta(\mathbf{r})\Delta(\mathbf{r}')\rangle \to C$, it vanishes in 2D structures because of destruction of the ODLRO by long wavelength fluctuations [72]. The vacancies in the graphene correlate according to powerlike interaction. Therefore, the vacancies form a cluster (hole) by joining each other, which competes with the 2D graphene structure. The vacancy-induced magnetism in the graphene is determined by the dangling bonds on the edge of the hole. On the other hand, the hole structure is energetically favorable when the dangling bonds on the edge

rebind to each other, reducing the magnetization to a minimal value. The graphene structure is destroyed by reaching the hole size to a critical value.

A graphene structure with randomly distributed vacancies can be considered as kinetically frozen in thermodynamically nonequilibrium states. A clustering of the vacancies into holes in a graphene sheet can be understood as a segregation of the structure, which means a partitioning of atomic or molecular constituents into macroscopic regions of different compositions. To understand segregation of vacancies in a graphene sheet, we study analytically dynamics of the carbon atoms and vacancies by means of nonlinear diffusion equations. Exact solution of these KdV-like nonlinear equations shows that the vacancies created in the middle of the sample diffuse to the boundary of the sample, resulting in a self-healing of the graphene layer.

ACKNOWLEDGMENTS

The reported study was funded by the Science Development Foundation under the President of the Republic Azerbaijan, Grant No EIF-KETPL-2-2015-1(25)-56/01/1, and partially by Azerbaijan-JINR collaboration. E.N. is grateful to Prof. V. A. Osipov for useful discussions.

[1] K. S. Novoselov, A. K. Geim, S. V. Morozov, D. Jiang, Y. Zhang, S. V. Dubonos, I. V. Grigoreva, and A. A. Firsov, Science **306**, 666 (2004).
[2] A. K. Geim, Science **324**, 1530 (2009).
[3] K. S. Novoselov, Z. Jiang, Y. Zhang, S. V. Morozov, H. L. Stormer, U. Zeitler, J. C. Maan, G. S. Boebinger, P. Kim, and A. K. Geim, Science **315**, 1379 (2007).
[4] J. H. Warner, M. H. Rümmel, L. Ge, T. Gemming, B. Montanari, N. M. Harrison, B. Büchner, and G. A. D. Briggs, Nat. Nanotech. **4**, 500 (2009).
[5] R. Zhao, J. Zhuang, Z. Liang, T. Yan, and F. Ding, Nanoscale **7**, 8315 (2015).
[6] R. Zan, U. Bangert, Q. Ramasse, and K. S. Novoselov, J. Phys. Chem. Lett. **3**, 953 (2011).
[7] Q. M. Ramasse, R. Zan, U. Bangert, D. W. Boukhvalov, Y.-W. Son, and K. S. Novoselov, ACS Nano **6**, 4063 (2012).
[8] B. W. Smith and D. E. Luzzi, J. Appl. Phys. **90**, 3509 (2001).
[9] R. Zan, Q. M. Ramasse, U. Bangert, and K. S. Novoselov, Nano Lett. **12**, 3936 (2012).
[10] J. Chen, T. Shi, T. Cai, T. Xu, L. Sun, X. Wu, and D. Yu, Appl. Phys. Lett. **102**, 103107 (2013).
[11] X. Gao, L. Liu, S. Irle, and S. Nagase, Angew. Chem., Int. Ed. Engl. **49**, 3200 (2010).
[12] L. Wang, F. Yan, H. L. W. Chan, and F. Ding, Nanoscale **4**, 7489 (2012).
[13] A. Santana, A. M. Popov, and E. Bichoutskaia, Chem. Phys. Lett. **557**, 80 (2013).
[14] T. Botari, R. Paupitz, P. A. Autrero, and D. S. Galvao, Carbon **99**, 302 (2016).
[15] Z. Liu, Y.-C. Lin, C.-C. Lu, C.-H. Yeh, P.-W. Chiu, S. Iijima, and K. Suenaga, Nat. Commun. **5**, 4055 (2014).
[16] V. O. Ozcelik, H. H. Gurel, and S. Ciraci, Phys. Rev. B **88**, 045440 (2013).
[17] P. T. Araujo, M. Terrones, and M. S. Dresselhaus, Mater. Today **15**, 98 (2012).
[18] G. Mestl, N. I. Maksimova, N. Keller, V. V. Roddatis, and R. Schlögl, Angew. Chem., Int. Ed. Engl. **40**, 2066 (2001).
[19] J. M. Carlsson and M. Scheffler, Phys. Rev. Lett. **96**, 046806 (2006).
[20] M. M. Ugeda, I. Brihuega, F. Guinea, and J. M. Gómez-Rodríguez, Phys. Rev. Lett. **104**, 096804 (2010).
[21] Y. Wang, Y. Huang, Y. Song, X. Zhang, Y. Ma, J. Liang, and Y. Chen, Nano Lett. **9**, 220 (2009).
[22] J. Ćervenka, M. I. Katsnelson, and C. F. J. Flipse, Nat. Phys. **5**, 840 (2009).
[23] O. V. Yazyev and L. Helm, Phys. Rev. B **75**, 125408 (2007).
[24] J. J. Palacios and F. Ynduráin, Phys. Rev. B **85**, 245443 (2012).
[25] S. Chakrabarty, A. H. M. Abdul Wassey, R. Thara, and G. P. Das, AIP Adv. **5**, 087163 (2015).
[26] O. V. Yazyev, Rep. Prog. Phys. **73**, 056501 (2010).
[27] Y. Zhang, S. Talapatra, S. Kar, R. Vajtai, S. K. Nayak, and P. M. Ajayan, Phys. Rev. Lett. **99**, 107201 (2007).
[28] F. Banhart, J. Kotakoski, and A. Krasheninnikov, ACS Nano **5**, 26 (2011).
[29] Y. Ma, P. O. Lehtinen, A. S. Foster, and R. M. Nieminen, New J. Phys. **6**, 68 (2004).
[30] X. Y. Cui, R. K. Zheng, Z. W. Liu, L. Li, B. Delley, C. Stampfl, and S. P. Ringer, Phys. Rev. B **84**, 125410 (2011).
[31] V. M. Pereira, J. M. B. Lopes dos Santos, and A. H. Castro Neto, Phys. Rev. B **77**, 115109 (2008).
[32] V. M. Pereira, F. Guinea, J. M. B. Lopes dos Santos, N. M. R. Peres, and A. H. Castro Neto, Phys. Rev. Lett. **96**, 036801 (2006).
[33] P. Ruffieux, O. Gröning, P. Schwaller, L. Schlapbach, and P. Gröning, Phys. Rev. Lett. **84**, 4910 (2000).
[34] H. A. Mizes and J. S. Foster, Science **244**, 559 (1989).
[35] P. Ruffieux, M. Melle-Franco, O. Gröning, M. Bielmann, F. Zerbetto, and P. Gröning, Phys. Rev. B **71**, 153403 (2005).
[36] E. H. Lieb, Phys. Rev. Lett. **62**, 1201 (1989).
[37] M. Slota, A. Keerthi, W. K. Myers, E. Tretyakov, M. Baumgarten, A. Ardavan, H. Sadeghi, C. J. Lambert, A. Narita, K. Müller, and L. Bogani, Nature **557**, 691 (2018).
[38] R. R. Nair, M. Sepioni, I.-L. Tsai, O. Lehtinen, J. Keinonen, A. V. Krasheninnikov, T. Thomson, A. K. Geim, and I. V. Grigorieva, Nat. Phys. **8**, 199 (2012).
[39] R. R. Nair, I.-L. Tsai, M. Sepioni, O. Lehtinen, J. Keinonen, A. V. Krasheninnikov, A. H. Casto Neto, M. I. Katsnelson, A. K. Geim, and I. V. Grigorieva, Nat. Commun. **4**, 2010 (2013).
[40] M. Sepioni, R. R. Nair, S. Rablen, J. Narayanan, F. Tuna, R. Winpenny, A. K. Geim, and I. V. Grigorieva, Phys. Rev. Lett. **105**, 207205 (2010).
[41] T. R. Anthony, in *Radiation Induced Voids in Metals and Alloys*, edited by J. W. Corbett and L. C. Ianiello, AEC Symp. Series, Conf-701601 (U.S.A.E.C. Technical Information Center, Oak Ridge, Tennessee, 1972), p. 630.
[42] P. R. Okamoto, S. D. Harkness, and J. J. Laidler, ANS Trans. **16**, 70 (1973).

[43] P. R. Okamoto and S. D. Harkness, Quarterly Prog. Report, HEDL-TME-72-144 (August, September, October 1972).
[44] P. R. Okamoto, A. T. Santhanam, H. Wiedersich, and A. Taylor, Nucl. Technol. **22**, 45 (1974).
[45] A. T. Santhanam, A. Taylor, and S. D. Harkness, in *Proceedings of the International Conference on Defects and Defect Clusters in BCC Metals and Their Alloys*, edited by R. J. Arsenault, Nuclear Metallurgy Vol. 18 (National Bureau of Standards, Gaithersburg, MD, 1973), p. 302.
[46] P. R. Okamoto and H. Wiedersich, J. Nucl. Math. **53**, 336 (1974).
[47] R. A. Johnson and N. Q. Lam, Phys. Rev. B **13**, 4364 (1976).
[48] R. A. Johnson and N. Q. Lam, Phys. Rev. B **15**, 1794 (1977).
[49] L. E. Rehn, P. R. Okamoto, D. I. Potter, and H. Wiedersich, J. Nucl. Math. **74**, 242 (1978).
[50] R. A. Johnson and N. Q. Lam, J. Nucl. Mater. **69 & 70**, 424 (1978).
[51] H. Wiedersich, P. R. Okamoto, and N. Q. Lam, J. Nucl. Mater. **83**, 98 (1979).
[52] P. Ordejón, E. A. Artacho, and J. M. Soler, Phys. Rev. B **53**, R10441 (1996).
[53] J. M. Soler, E. Artacho, J. D. Gale, A. Garcia, J. Junquera, P. Ordejón, and D. Sanchez-Portal, J. Phys. C **14**, 2745 (2002).
[54] J. P. Perdew, K. Burke, and M. Ernzerhof, Phys. Rev. Lett. **77**, 3865 (1996).
[55] H. J. Monkhorst and J. D. Pack, Phys. Rev. B **13**, 5188 (1976).
[56] A. A. El-Barbary, R. H. Telling, C. P. Ewels, M. I. Heggie, and P. R. Briddon, Phys. Rev. B **68**, 144107 (2003).
[57] A. V. Krasheninnikov, P. O. Lehtinen, A. S. Foster, and R. M. Nieminen, Chem. Phys. Lett. **418**, 132 (2006).
[58] P. A. Thrower and R. M. Mayer, Phys. Status Solidi A **47**, 11 (1978).
[59] A. J. Stone and D. J. Wales, Chem. Phys. Lett. **128**, 501 (1986).
[60] Y. Kim, J. Ihm, E. Yoon, and G.-D. Lee, Phys. Rev. B **84**, 075445 (2011).
[61] T. Trevethan, C. D. Latham, M. I. Heggie, P. R. Briddon, and M. J. Rayson, Nanoscale **6**, 2978 (2014).
[62] A. Hashimoto, K. Suenaga, A. Gloter, K. Urita, and S. Iijima, Nature **430**, 870 (2004).
[63] J. C. Meyer, C. Kisielowski, R. Erni, M. D. Rossel, M. F. Grommie, and A. Zettl, Nano Lett. **8**, 3582 (2008).
[64] C. Ö. Girit, J. C. Meyer, R. Erni, M. D. Rossell, C. Kisielowski, L. Yang, C.-H. Park, M. F. Grommie, M. L. Cohen, S. G. Louie, and A. Zettl, Science **323**, 1705 (2009).
[65] O. Lehtinen, I.-L. Tsai, R. Jalil, R. R. Nair, J. Keinonen, U. Kaiser, and I. V. Grigorieva, Nanoscale **6**, 6569 (2014).
[66] L. Tapaszto, G. Dobrik, P. Nemes-Incze, G. Vertesy, Ph. Lambin, and L. P. Biró, Phys. Rev. B **78**, 233407 (2008).
[67] G. D. Lee, C. Z. Wang, E. Yoon, N. M. Hwang, D. Y. Kim, and K. M. Ho, Phys. Rev. Lett. **95**, 205501 (2005).
[68] M. Saito, K. Yamashita, and T. Oda, Jpn. J. Appl. Phys. **46**, L1185 (2007).
[69] The multiplayer $1/6$ in the front of d_{AV} and d_{Ai} in Ref. [51], which is valid for 3D systems is replaced by $1/4$ according to Fick's diffusion coeffisient for 2D systems.
[70] P. G. Drazin and R. S. Johnson, *Solitons: An Introduction* (Cambridge Text in Applied Mathematics, Cambridge, 1989).
[71] N. D. Mermin and H. Wagner, Phys. Rev. Lett. **17**, 1133 (1966).
[72] T. M. Rice, Phys. Rev. **140**, A1889 (1965).